Gold Nanoparticles Interacting with β-Cyclodextrin–Phenylethylamine Inclusion Complex: A Ternary System for Photothermal Drug Release

Rodrigo Sierpe,[†,‡,∥] Erika Lang,[‡] Paul Jara,[‡] Ariel R. Guerrero,[†,∥] Boris Chornik,[§] Marcelo J. Kogan,*[,†,∥] and Nicolás Yutronic*[,‡]

[†]Departamento de Química Farmacológica y Toxicológica, Facultad de Ciencias Químicas y Farmacéuticas, Universidad de Chile, Sergio Livingstone #1007, Independencia, Santiago, Chile

[‡]Departamento de Química, Facultad de Ciencias, Universidad de Chile, Las Palmeras #3425, Ñuñoa, Santiago, Chile

[§]Departamento de Física, Facultad de Ciencias Físicas y Matemáticas, Universidad de Chile, Beauchef #850, Santiago, Chile

[∥]Advanced Center for Chronic Diseases (ACCDiS), Sergio Livingstone #1007, Independencia, Santiago, Chile

S *Supporting Information*

ABSTRACT: We report the synthesis of a 1:1 β-cyclodextrin–phenylethylamine (βCD-PhEA) inclusion complex (IC) and the adhesion of gold nanoparticles (AuNPs) onto microcrystals of this complex, which forms a ternary system. The formation of the IC was confirmed by powder X-ray diffraction and NMR analyses (^{1}H and ROESY). The stability constant of the IC (760 M^{-1}) was determined using the phase solubility method. The adhesion of AuNPs was obtained using the magnetron sputtering technique, and the presence of AuNPs was confirmed using UV–vis spectroscopy (surface plasmon resonance effect), which showed an absorbance at 533 nm. The powder X-ray diffractograms of βCD-PhEA were similar to those of the crystals decorated with AuNPs. A comparison of the one- and two-dimensional NMR spectra of the IC with and without AuNPs suggests partial displacement of the guest to the outside of the βCD due to attraction toward AuNPs, a characteristic tropism effect. The size, morphology, and distribution of the AuNPs were analyzed using TEM and SEM. The average size of the AuNPs was 14 nm. Changes in the IR and Raman spectra were attributed to the formation of the complex and to the specific interactions of this group with the AuNPs. Laser irradiation assays show that the ternary system βCD-PhEA-AuNPs in solution enables the release of the guest.

Formation of the ternary system βcyclodextrin-Drug-AuNPs in solid state.

Drug release in solution by photothermal effect.

KEYWORDS: *inclusion complex, β-cyclodextrin, phenylethylamine, gold nanoparticles, magnetron sputtering, photothermal effect*
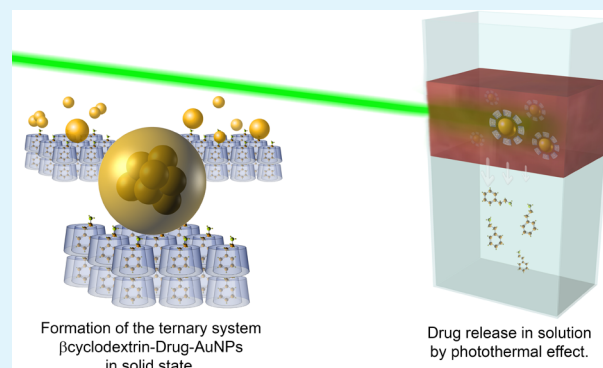
1. INTRODUCTION

Cyclodextrins (CDs) are nontoxic cyclic oligosaccharides formed from glucopyranose units bonded via $\alpha(1{-}4)$ bonds as a truncated cone (Figure 1a) with an apolar internal cavity and a polar external surface. Several weak forces, including hydrophobic van der Waals forces, dipole–dipole interactions and hydrogen-bonding interactions cooperatively determine the behavior of CDs as a matrix in the inclusion complex (IC). The three most common forms are α-, β-, and γ-CDs, which are composed of six, seven, and eight glucose units, respectively. Due to the particular molecular structure with a hydrophobic internal cavity and hydrophilic outer surface, CDs preferentially include nonpolar compounds, such as aliphatic or cyclic hydrocarbons.[1–5] β-Cyclodextrin (βCD) is the least expensive, most accessible, and generally the most useful CD, and is used especially to include molecules with aromatic rings in its structure.[6–9] βCD has numerous pharmacological applications;

for example, it increases the water solubility and decreases the toxicity of many substances by forming complexes. In this manner, the bioavailability of drugs is increased, allowing to decrease the drug dose; moreover, the included drugs placed as guests may be transported within the organism to the target site of action and released uniformly over time.[5,10–18] The applications of CDs in various drug formulations have been extensively investigated and brought to market. For example, βCD was approved by the United States Food and Drug Administration (FDA) in 2001, thereby enabling its use in the food industry, cosmetology, and clinical applications in humans. In 2008, CDs experienced strong growth; six products were approved by the FDA, approximately 600 patents and
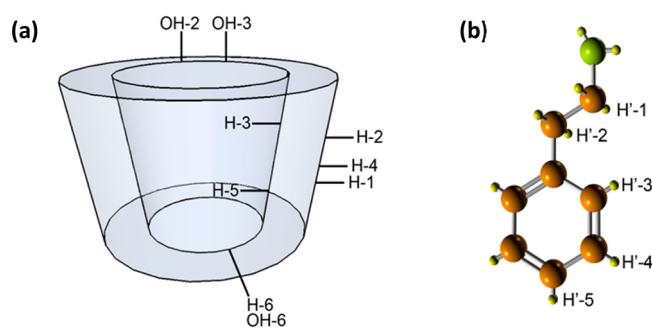
(a)

(b)

Figure 1. Detailed schematic of the assignment of protons of (a) βCD and (b) PhEA.

applications on drug formulations were published, and over 500 scientific articles included CDs in their studies. Currently, the contributions of βCD and its derivatives continue to increase, and new systems have been developed. The use of hydroxypropyl-βCD in Niemann-Pick type C disease and CDs in polymeric form or gold nanoparticles (AuNPs) with coupled CDs for the transportation of antitumor drugs are some of its applications. The vast number of patents and published research articles and the constant development of new strategies for drug delivery using CDs show the extent of this field within the pharmaceutical industry.[5,13,14,19−25]

Phenylethylamine (PhEA; Figure 1b) is a psychoactive stimulant that produces effects such as wakefulness, arousal, and tachycardia, and it is employed as an antidepressant. It is an endogenous neuroamine, with similar effects to amphetamines without inducing tolerance; however, despite its favorable properties, it is rapidly metabolized in the organism via the MAO-B enzyme and does not reach the brain in significant concentrations. PhEA exhibits high lipid solubility; thus, it is an attractive drug for improving its water solubility and preventing its rapid degradation via inclusion in cyclodextrins.[26−29]

Moreover, metal nanoparticles (MNPs) possess many attractive properties, including optical, electronic, and magnetic properties, among others. The properties of MNPs depend not only on their size but also on their morphology and spatial arrangement. The effects described above produce a direct impact on the surface properties and chemical reactivity of nanostructured systems.[30−35] Nanoparticle systems are extensively investigated for drug delivery[36−39] and could be applied in the treatment of diseases associated with inflammation and tumors. In such pathological conditions, the endothelial lining of the blood vessel wall becomes more permeable than in the normal state of the tissue, allowing the selective accumulation of nanoparticles, known as the enhanced permeability and retention (EPR) effect. Consequently, certain nanoparticles ranging from 10 to 500 nm in size can leave the vascular bed and accumulate inside the interstitial space, allowing a passive targeting of active drugs associated with them.[40−43] Furthermore, a certain proportion of these systems can cross the blood-brain barrier and reach the brain, as it has been demonstrated for AuNPs.[44−46]

AuNPs in drug-delivery systems show several interesting characteristics, including high solubility, high stability in living systems, capacity for biodistribution, and improved kinetics for drug distribution. They can form nanoreservoirs for sustained delivery with controlled distribution of the drug in order to keep it within the therapeutic window.[47−50] Moreover, it has been reported that gold nanospheres between 4 and 100 nm do

not show any apparent cytotoxic effects, in contrast to smaller gold nanospheres that are highly toxic.[51−54] The properties of AuNPs may be modified by functionalization with ligands to obtain optimized nanosystems for various therapeutic applications.[44,45,55−57] These ligand molecules have to be bound to the particle surface by some attractive interaction, such as chemisorption or electrostatic attraction, among others.[30,58−60]

Studies performed primarily by our research group have demonstrated that AuNPs can be deposited onto inclusion complexes of cyclodextrins using organic molecules as guest and that possess functional groups such as thiol, carboxylic acid or amine groups.[61−65] Additionally, due to the plasmon effect of AuNPs, it is possible to promote photothermally controlled drug release. AuNPs possess what is termed a localized surface plasmon resonance, where the collective oscillation of the electrons in the surface of the metal occurs due to interaction with light. The absorbed energy is dissipated as local heat, which could be used for photothermal drug release.[66−69] In the context of clinical applications of AuNPs, it is important to note that their uses are still incipient. At present, there are some applications of AuNPs for therapy; however, many of these treatments exist only in the clinical trial phase.[70] One example in clinical phase II is the potential use of AuNPs labeled with recombinant human tumor necrosis factor alpha (TNF-α) for the targeting of solid tumors in advanced stage cancer patients.[71]

In order to develop a method for a controlled drug delivery, we studied a system containing AuNPs and βCD. The use of various cyclodextrins for the synthesis of AuNPs has been previously reported.[72−74] Furthermore, numerous nanometric systems have been designed, in which AuNPs are covered by modified CDs for potential biological applications.[23−25,75−77]

In this work, a ternary system containing an active drug (PhEA) and two components (βCD and AuNPs) that would allow spatially and temporally controlled drug release was obtained. This ternary system was formed using βCD as a matrix, PhEA as a guest and AuNPs on crystals of IC. The nanoparticles were deposited by magnetron sputtering. The ternary system was characterized using powder X-ray diffraction, NMR, UV−vis, TEM, SEM, EDX, IR, and SERS. The stability constants and the photothermal release of PhEA were studied.

2. EXPERIMENTAL PROCEDURES

Materials. All chemicals were of analytical grade and were used without further purification. All aqueous solutions were prepared in purified water for chromatography. β-Cyclodextrin hydrate (98% purity) and phenylethylamine (99.5% purity, density 0.962 g/mL) were provided by the Aldrich Chemical Co.

Synthesis of the Inclusion Complex. The synthesis of βCD-PhEA was performed at a 1:1 molar ratio. A saturated solution of βCD (0.5 g) in water was formed with constant and homogeneous stirring at room temperature, and then 55.5 μL of PhEA was added. The mixture was maintained under gentle stirring for 1 h. The solution remained under a hood until a crystalline powder was obtained, which precipitated slowly after 48 h. The crystals were washed, filtered and dried under vacuum. The sample was pulverized to remove clusters.

Formation of Gold Nanoparticles. AuNPs were obtained by deposition as an epitaxial layer onto microcrystals of βCD-PhEA using a physical method called magnetron sputtering under high vacuum. To deposit the nanoparticles, a gold foil was used as a cathode and crystalline powder of the complex was used as a substrate inside a vacuum chamber at 0.5 mbar under an inert atmosphere of argon. A current of 25 mA was used to ionize the gas, thereby initiating the process. AuNPs were formed on the crystal faces of βCD-PhEA in 20

or 60 s of sputtering, forming the ternary system of βCD-PhEA-AuNPs.

Characterization of βCD-PhEA by Powder X-ray Diffraction (PXRD). The analysis was performed using a Siemens D-5000 diffractometer with graphite-monochromated Cu Kα radiation at 40 kV and 30 mA with a wavelength of 1.540598 Å.

Characterization of βCD-PhEA by NMR. ^{1}H NMR and ROESY measurements were performed at 300 K in DMSO-d_6 (99.99% D) on a Bruker Advance 400 MHz superconducting NMR spectrometer. All 2D NMR spectra were acquired using pulsed field gradient-selected methods. Additionally, the stoichiometry of the complex was evaluated using the integration of the signals of the protons of βCD and PhEA in the spectrum of βCD-PhEA.

Determination of Stoichiometry and Stability Constant of βCD-PhEA. The determination of the stoichiometry of the complex also was performed by the continuous variation method (Job's method) and the stability constant (K) of the complex in water was obtained via the solubility phase method using a PerkinElmer UV−vis Lambda 25 spectrophotometer (more details in the Supporting Information, sections S3 and S4).

Characterization of AuNPs Deposited onto βCD-PhEA. The ternary complex was first characterized by PXRD, ^{1}H NMR, and 2D NMR measurements using the above-described conditions.

UV−Vis Absorption Spectra of AuNPs. Solid samples of AuNPs on crystals of βCD-PhEA were characterized via diffuse reflectance measured using a Shimadzu UV 2450 spectrophotometer with barium sulfate as a baseline. Additionally, βCD-PhEA spectrum was used as a second baseline. The absorbance was determined based on Kubelka−Munk transformations.

Transmission Electron Microscopy (TEM). TEM was performed using a JEOL JEM 1200 EX II instrument. This instrument operates at low pressures, typically on the order of $10^{-4}-10^{-8}$ kPa. All samples were measured at an acceleration voltage of 80 kV. The samples were prepared by dispersing approximately 1.0 mg of the system in 1.0 mL of 30% isopropanol. Then, 10 μL of the solution was deposited onto a copper grid with a continuous film of Formvar, the excess solution was removed, and the grid was dried.

Scanning Electron Microscopy (SEM). SEM images were obtained using a LEO 1420VP system equipped with an Oxford 7424 energy dispersive spectrometer (EDS) at an accelerating voltage of 25 kV and a JEOL JIB4500 instrument.

IR and Raman Vibrational Spectroscopy. IR spectra for βCD-PhEA and βCD-PhEA-AuNPs were measured using a PerkinElmer System 2000 with KBr pellets, for βCD and PhEA using an Interspec 200-x FTIR spectrometer. Raman spectra were measured using a Renishaw Ramascope 1000 instrument, with the excitation of a He−Ne laser line of 632.8 nm, measuring directly from the powdered samples for βCD, βCD-PhEA, and βCD-PhEA-AuNPs, and from the liquid state for pure PhEA. For measurement of the βCD-PhEA-AuNPs, the laser power was reduced to 25% of that employed for the other samples. To interpret the results of the IR and Raman spectra, calculations with the PhEA molecule were performed using Gaussian 09, revision D.01[78] using density functional theory at the B3LYP/6-311+G(d,p) level of theory in the gaseous state. Geometry optimization and frequency calculations, including Raman activity, were requested.

Determination of Gold Content, CD, and PhEA in the Ternary System. The percentage of gold deposited on the βCD-PhEA crystalline powder was determined using a PinAAcle 900F atomic absorption spectrometer equipped with a double hollow cathode lamp (Au and Ag) and laminar flame. The percentages of βCD and PhEA were obtained from the mass fraction of each component in the systems and the matrix-guest stoichiometry (more details in the Supporting Information, section S7). The percentage of the PhEA in the ternary system in aqueous solution was determined using a PerkinElmer UV−vis Lambda 25 spectrophotometer (more details in the Supporting Information, section S8).

Laser Irradiation Assays. For irradiation assays, a continuous laser (Power Technology Inc.) at 532 nm, beam diameter of 1 mm and 45 mW of light power was used. First, a stock solution of βCD-PhEA-

AuNPs in water (concentration of 4.0 mg/mL) was prepared. A two-phase system was formed using quartz cuvettes with a chloroform solution, and then 150 μL of the aqueous solution of βCD-PhEA-AuNPs was added. The volume of the aqueous solution was exactly equal to the width of the laser beam such that the nanoparticles were completely excited by the light. AuNPs covered with the complex were exposed to laser irradiation for different time periods. Without separating the two phases, the absorbance of PhEA was measured solely in the chloroform phase using a UV−vis spectrophotometer. As a control, an aqueous solution of the βCD-PhEA complex (4.0 mg/mL) was prepared and used for studies of laser irradiation without AuNPs. For the PhEA spectra in chloroform, the maximum values of absorbance obtained at a wavelength of 258 nm were converted to percentages and were compared with the maximum absorbance corresponding to the total PhEA aggregated in the system. The absorbance curve for the maximum PhEA was obtained by directly dissolving an equivalent amount of drug that is present in the stock solution of βCD-PhEA-AuNPs in chloroform.

3. RESULTS AND DISCUSSION

Confirmation of Complex Formation in the Solid State. When a diffractometric trace of a crystal differs from another based on the disappearance of characteristic peaks and the appearance of new peaks, complex formation is considered "very likely" because the crystal packing arrangement of the IC is generally different from the peaks of the original species.[79,80] This may be analyzed using powder X-ray diffraction (Figure 2). For βCD-PhEA (trace b), some peak variations appeared
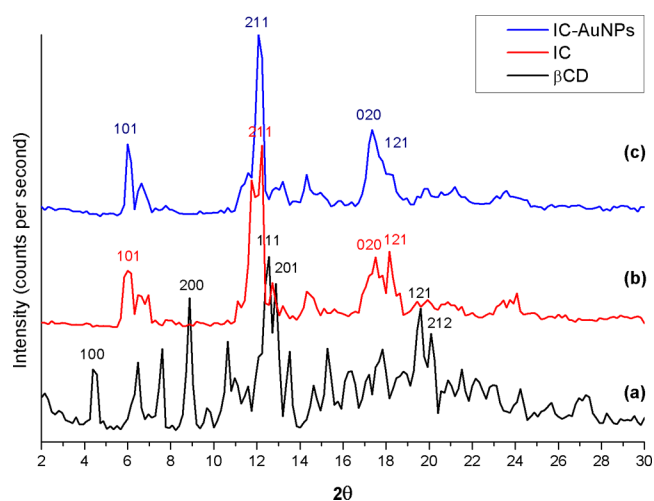

Figure 2. Diffractograms of crystals of (a) β-cyclodextrin, pure and without guest; (b) βCD-PhEA complex; and (c) βCD-PhEA-AuNPs complex.

compared with the diffractogram of pure βCD (trace a). The differences in the diffractograms were due to the entry of PhEA into the cyclodextrin cavity with the production of a new crystalline structure. Intense peaks observed at the angles of approximately 6°, 12° and 18° for 2θ correspond to the common diffraction peaks of βCD with a guest that contains a benzene ring included in the internal cavity.[6,79−81] The systems were indexed to the monoclinic P2₁ space group (more details in the Supporting Information, section S1). The formation of nanostructures by deposition is a process governed by the arrangement of the functional groups on the microcrystal surface, a phenomenon called *crystal lattice mediated self-assembly* (CLAMS).[82−84] A high degree of crystallinity of the βCD-PhEA complex was demonstrated, forming a suitable

surface for stabilizing AuNPs. Furthermore, the characteristic peaks in the IC diffractogram did not vary when metal nanoparticles were added, as shown in trace c (Supporting Information, section S1).

Confirmation of the Presence of the Complex in Solution. NMR is one of the most efficient techniques for studying molecular interactions. Based on the chemical shifts of protons of the aromatic ring and of the ethylamine chain (Figure 1b), the complex formation may be analyzed for PhEA. For βCD, protons 1, 2, and 4 are located on the outside surface, and protons 3 and 5 are located within the cavity (Figure 1a). Protons 3 are near the wide aperture, and protons 5 are located near the narrow aperture. Protons 6 are located in the lower cavity surface.[3] The ^{1}H NMR spectra of pure species, matrix, and guest show distinct signals that did not overlap, even when forming the IC; thereby, it is possible to evaluate the chemical shifts of their spectra (Supporting Information, section S2). Chemical shift data for free PhEA, free βCD, and the inclusion complex are shown in Table 1. These values indicate that the

Table 1. ^{1}H NMR Chemical Signals of the Host, Guest, and Inclusion Compound and Their Corresponding Displacements ($\Delta\delta$)

H of the matrix	δ βCD (ppm)	δ βCD-PhEA (ppm)	$\Delta\delta$ (ppm)
H-1	4.826	4.825	−0.001
H-3	3.669	3.656	−0.013
H-5	3.566	3.556	−0.010
H-6	3.622	3.610	−0.012
OH-2	5.707	5.753	0.046
OH-3	5.660	5.707	0.047
OH-6	4.435	4.473	0.038
H of the guest	δ PhEA (ppm)	δ βCD-PhEA (ppm)	$\Delta\delta$ (ppm)
H′-1	2.795	2.750	−0.045
H′-2	2.658	2.628	−0.030
H′-3	7.205	7.197	−0.008
H′-4	7.285	7.276	−0.009
H′-5	7.176	7.169	−0.007

protons of the aromatic ring of the guest change their chemical shifts when the complex is formed, as for the internal protons of the βCD molecule. Chemical shifts were observed for all signals of PhEA toward higher fields because the interactions with the cavity restrict the space of the protons of the guest, providing a higher electron density in its environment. With respect to the matrix, evidence suggested that the IC was formed due to the shielding of H-3, H-5, and H-6 produced by the electronic contribution of the aromatic ring. Since PhEA remains inside the matrix, the hydroxyl groups show different interactions. Protons OH-2, OH-3, and OH-6 are affected by the proximity of the electronegative amine group and by the deshielding effect of the aromatic current.

Stoichiometry and Stability of the IC. A 1:1 stoichiometry for the complex was determined by two methods. On the one hand, using the integration of H-1 of the matrix as a reference and comparing it with the protons of the ethylamine chain in the spectra of NMR of βCD-PhEA with and without AuNPs according with the methodology used in different complexes of cyclodextrins.[62−85] On the other hand, using the continuous variation method via the absorbance of PhEA in assays with different concentrations of βCD[86] (Supporting Information, section S3).

The stability constant of the IC was determined via UV−vis following the methodology described by Higuchi and Connors.[52,87] Using the reported mathematical analyses, the constant K was found to be 760 M^{-1} (Supporting Information, section S4). These values are suitable for inclusion complexes of drugs for biological applications. The most common pharmaceutical uses of cyclodextrins are to enhance the solubility, stability, safety and bioavailability of the drugs, for this it is necessary a favorable formation reaction of the CD-drugs complexes with appropriate values of its stability constants. Generally, the K values of complexes of cyclodextrins vary between 50 and 2000 M^{-1}, due on the one hand that at lower values (<50 M^{-1}) the feasibility of a pharmaceutical formulation can be limited by its low stability which no favor a controlled release (for example, in the blood and not in the desired tissue). On the other hand, with high values (>2000 M^{-1}) the reaction rates can be affected by the high degree of inclusion of the drug into the cyclodextrin cavity avoiding the release, among other factors.[88,89]

Permanence of the Complex in Solution with AuNPs. ^{1}H NMR analysis of βCD-PhEA-AuNPs was performed. Changes in the chemical shifts with respect to pure species and the inclusion complex without AuNPs were observed (Supporting Information, section S2). Notably, the interaction of AuNPs with the amine group of PhEA produced differences in the signals, indicating a variation in the inclusion phenomenon due to a chemisorption process on the gold surface; nevertheless, the IC remained stable. All PhEA signals appeared toward higher fields, similar to the complex without AuNPs. The greater difference was in the internal protons of βCD, where the guest adopted a new internal arrangement. To study the disposition of the guest in the cavity of βCD, a 2D NMR analysis was performed. According to the ^{1}H NMR analysis of the βCD-PhEA-AuNPs, it is possible to confirm that the ternary system was stable in solution but that the arrangement of the guest PhEA was different with respect to the βCD-PhEA complex in the absence of AuNPs. The stoichiometric ratio between βCD and PhEA in the presence of AuNPs was still 1:1 (Supporting Information, section S3), which is relevant for assays of drug release.

Elucidation of Inclusion Geometry. For a more precise analysis of the inclusion phenomenon, we performed a ROESY examination, which enables the analysis of interactions between hydrogen nuclei, thereby between protons of cyclodextrins and organic molecules that are located at a maximum distance of 5 Å.[6,90] The 2D ROESY spectrum confirmed the formation of the IC and could determine the exact arrangement of the guest inside the βCD cavity.[8,91−96] In Figure 3a and b, it is possible to observe the cross peaks produced by the interaction of the aromatic ring protons and of the ethylamine chain protons of PhEA with protons H-3, H-5, and H-6 of βCD. Specifically, the intensity of the cross peaks showed a higher correlation between protons of the ethyl chain with protons H-6 of the matrix and between protons of the aromatic ring with internal protons H-5 and H-6 of βCD, indicating that the ethyl chain was oriented toward the narrower opening of the cavity.

Evidence of the interaction of the AuNPs with the complex βCD-PhEA is detailed in Figure 3c and d. Changes in the intermolecular correlations of the internal protons of βCD and protons of PhEA indicate a change in the inclusion phenomenon. The cross peak analysis shows that the ethylamine chain is partially out of the βCD cavity because it is interacting solely with H-6 (Figure 3c), whereas the aromatic
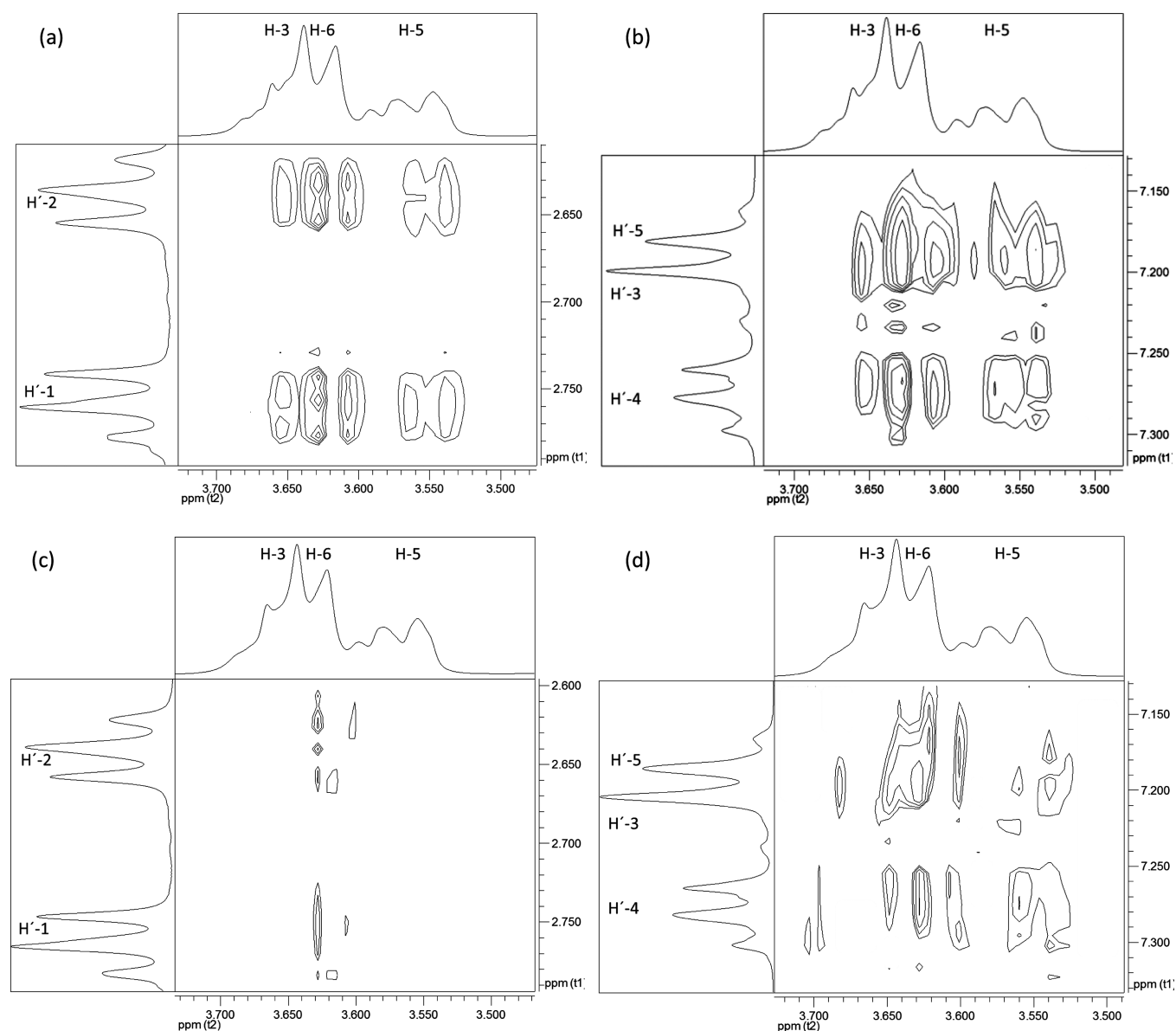
Figure 3. ROESY spectra: (a, b) H-3, H-5, and H-6 of βCD with protons H′-1, H′-2, H′-3, H′-4, and H′-5 of PhEA; (c, d) H-3, H-5, and H-6 of βCD with protons H′-1, H′-2, H′-3 H′-4, and H′-5 of PhEA in the presence of AuNPs.

ring remained inside (Figure 3d). For PhEA, the correlation of the protons of the aromatic ring with protons H-3 of βCD is less intense than the intermolecular correlation of the ring with protons H-5 and H-6 of βCD. This finding implies partial displacement of the guest toward the outside of the βCD via the narrowest opening of the cavity, which may be explained by the competition between the trend toward the inclusion of the guest via hydrophobic interaction with the cavity of the matrix and the attraction generated by the AuNPs interacting with the NH$_2$ functional group of PhEA.

Based on analysis of the ROESY spectra, Figure 4 shows a scheme of the complex formed (left) and the partial displacement of the guest to the outside of the βCD cavity due to the presence of AuNPs (right). This result is important to understand the permanence of the ternary system in solution, the ethylamine chain of PhEA remains outside the CD cavity, which is necessary to maintain the chemisorbed of NH$_2$ on the gold surface. On the other hand, the aromatic ring is
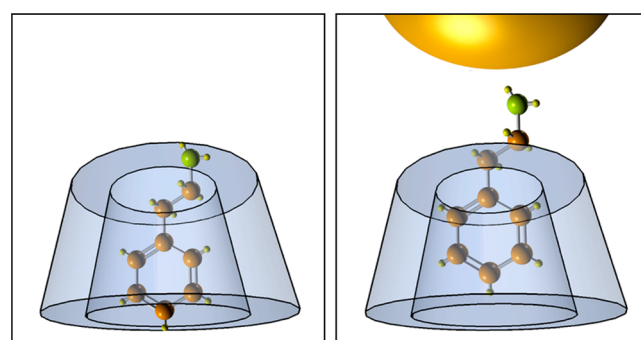

Figure 4. Proposed inclusion geometry for the complex βCD-PhEA without (left) and with AuNPs (right).

retained in the CD cavity, which shows that the complex remains stable.

UV−Vis Absorption Spectra of AuNPs on IC Crystalline Powder. Spherical AuNPs of 10−20 nm in diameter

exhibit a plasmon band with an absorption maximum at 520 nm.[33] Figure 5a presents the absorption spectrum of spherical
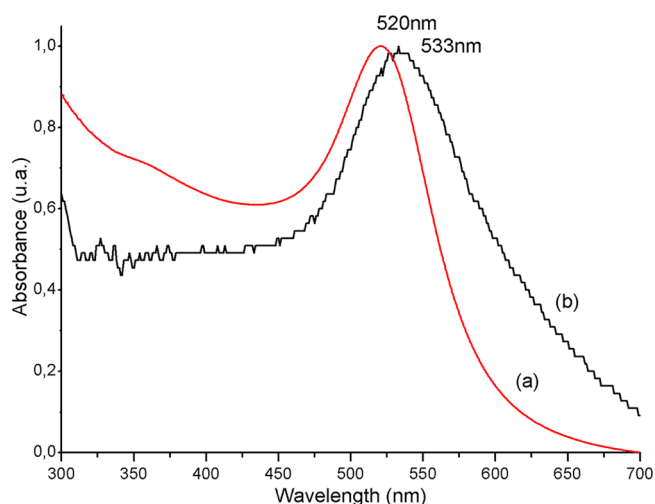

Figure 5. (a) Optical spectrum of AuNPs covered with citrate and (b) optical spectrum of AuNPs on microcrystal of the ICs.

particles of 10 nm in diameter in a colloidal solution of AuNPs capped with citrate. Spectrum b shows the surface plasmon resonance effect of spherical AuNPs onto IC crystals with an absorption maximum at 533 nm. The displacement of the band may be due to the larger size of these nanostructures, due to the change in the surrounding medium, even when metal nanoparticles are supported in a substrate, or also due to the phenomenon of interparticle coupling caused by the increased proximity between AuNPs in the solid state.[30−35]

Characterization of βCD-PhEA-AuNPs by TEM and SEM. Crystalline powder of the βCD-PhEA complex with AuNPs forming the ternary system was dissolved, and the AuNPs covered with IC were observed by TEM (Figure 6). The AuNPs were determined to be approximately 14 nm in diameter based on a statistical analysis (taking into account approximately 2600 nanoparticles) of the TEM image (more images in Supporting Information, section S5). These sizes are suitable for drug delivery purposes such as the possible crossing of biological barriers.[44−46,50]
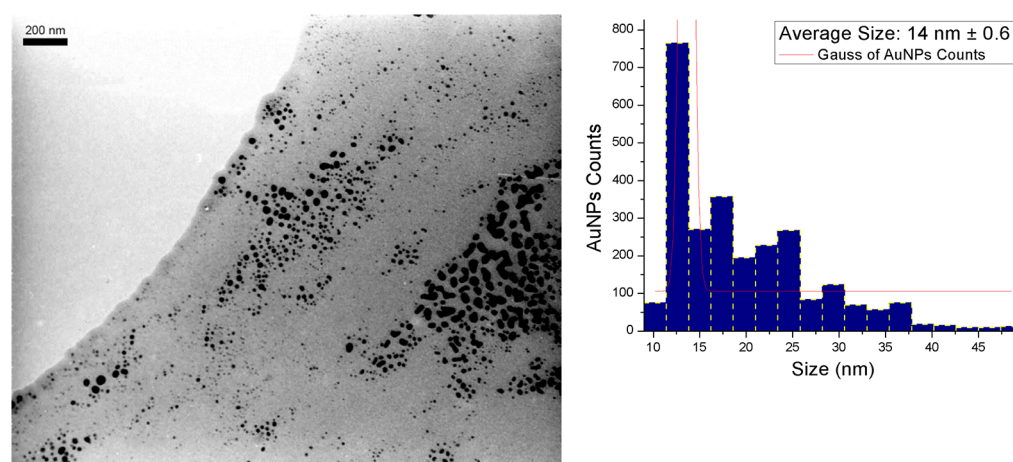
SEM images (Figure 7) showed that the structure of βCD-PhEA microcrystals decorated with AuNPs was consistent with the PXRD results. The βCD with its planar structure of a heptagon can form a parallelogram, which is one of the reasons why these complexes tend to form a monoclinic structure.[79,80] The EDX analysis of the crystalline powder showed the presence of gold in the sample, in addition to the other elements that formed the IC.

On the other hand, the samples observed using FE-SEM showed a low quality due to the low conductivity of the organic sample (data not shown); however, after increasing the deposition time from 20 to 60 s, AuNPs with larger sizes were observed. The dark-field FE-SEM image (Figure 8) showed nanostructures on the surface of the crystal that were approximately 40 nm in diameter.

Using the deposition method of nanoparticles by sputtering, it was possible to control the size of the AuNPs in function of the exposure time of crystals to this technique. Considering that the guest molecule (PhEA) in the IC remained exposed, the gold atoms released from the metal foil are retained in the substrate, initiating the epitaxial growth, which produces an increase in the size of the AuNPs when the sputtering times increase. Various chemical functional groups possess a certain affinity with gold surfaces, in this case the primary amines form partially covalent bonds with AuNPs; this interaction of the amines with gold is strong and similar with respect to thiolate bonds.[30,59,97,98] The metal nanoparticles were stabilized on the face surfaces of the crystals due to the CLAMS phenomenon that depends on the degree of ordering of the functional groups that are exposed on the surface.[62,82−84] In this regard, note that IC can stabilize different nanostructures, such as silver nanospheres, gold nanospheres and gold nanorods, by exposed functional groups on specific crystal faces.[61−65]

Study of the Interaction of AuNPs with the PhEA Molecules in the IC. The interaction between the matrix and the guest in the inclusion complex and the changes caused by the presence of AuNPs can be demonstrated by vibrational spectroscopy (IR and Raman). Commonly, these studies focus on the behavior of the traces of the guest molecule because the peaks of these molecules generally are shifted or their intensities are altered.[99−102] Figure 9 shows the IR spectra for (a) PhEA, (b) βCD, (c) βCD-PhEA, and (d) βCD-PhEA-AuNPs, where compared to the pure species, some signal
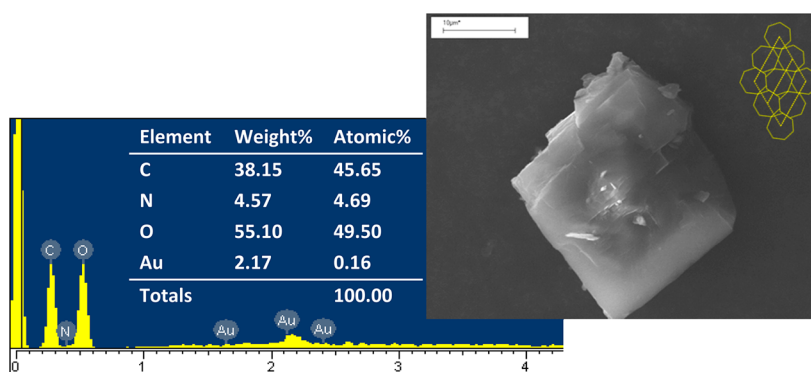

Figure 6. TEM image of AuNPs obtained by sputtering and their histogram.

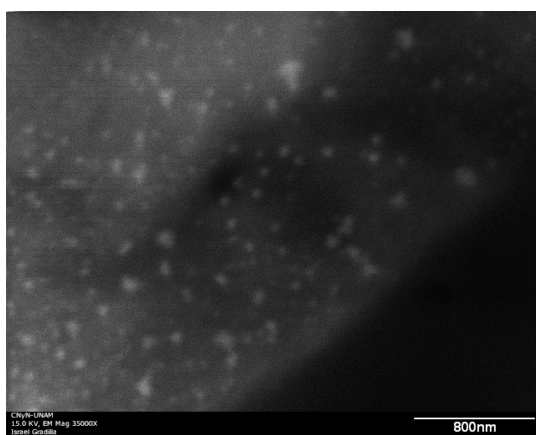**Figure 7.** SEM image of a crystal of βCD-PhEA and EDX analysis.

Figure 8. FE-SEM image of a side of a crystal of βCD-PhEA with AuNPs.

changes in the inclusion complex with or without AuNPs were observed.

For the PhEA spectrum, the major peaks observed were 592 cm^{-1}, corresponding to the aromatic ring deformation; 744 and 698 cm^{-1}, corresponding to the wagging of the aromatic ring; 1318 cm^{-1}, corresponding to the twisting of the ethyl chain; 1360 cm^{-1}, corresponding to the C−H bending of the aromatic ring; and 1495 cm^{-1}, corresponding to the C−H deformation of the aromatic ring, which disappears in the spectrum of the βCD-PhEA complex and the complex with AuNPs, probably due to the inclusion of PhEA into the βCD, where the aromatic ring loses some freedom of movement, similar to a phenomenon observed by Pandian et al.[100]

In addition, in the PhEA spectrum, a peak at 1030 cm^{-1}, corresponding primarily to the twisting of the ethyl chain, remained in the spectra of the βCD-PhEA complex with and without AuNPs. The C−N stretching at 1082 cm^{-1} remained in the spectrum of the βCD-PhEA complex and disappeared for this complex with the presence of AuNPs. The peak at 1453 cm^{-1} corresponding to the CH$_2$ wagging and C−N bending disappeared in the βCD-PhEA spectrum. In the βCD-PhEA-AuNPs, this last peak reappeared with a low intensity, probably
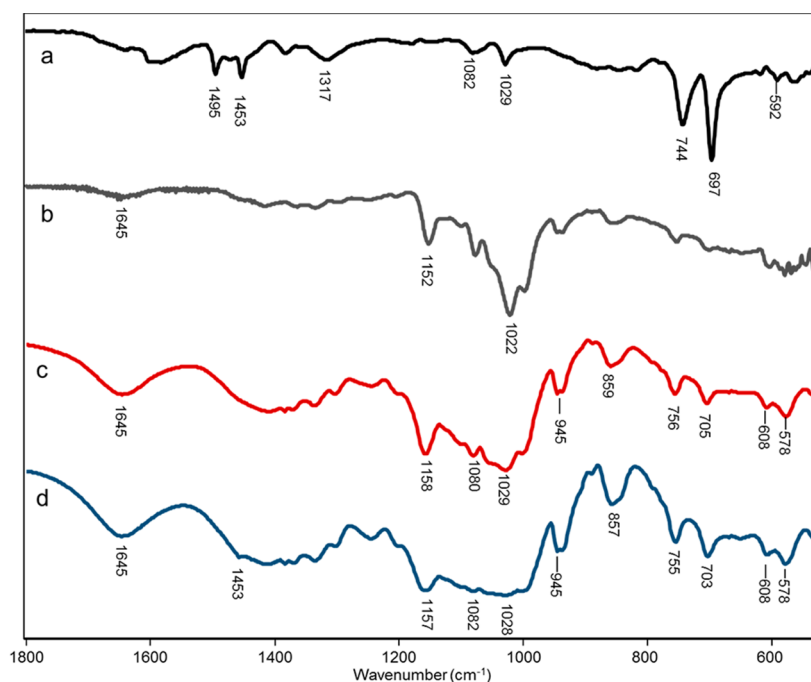

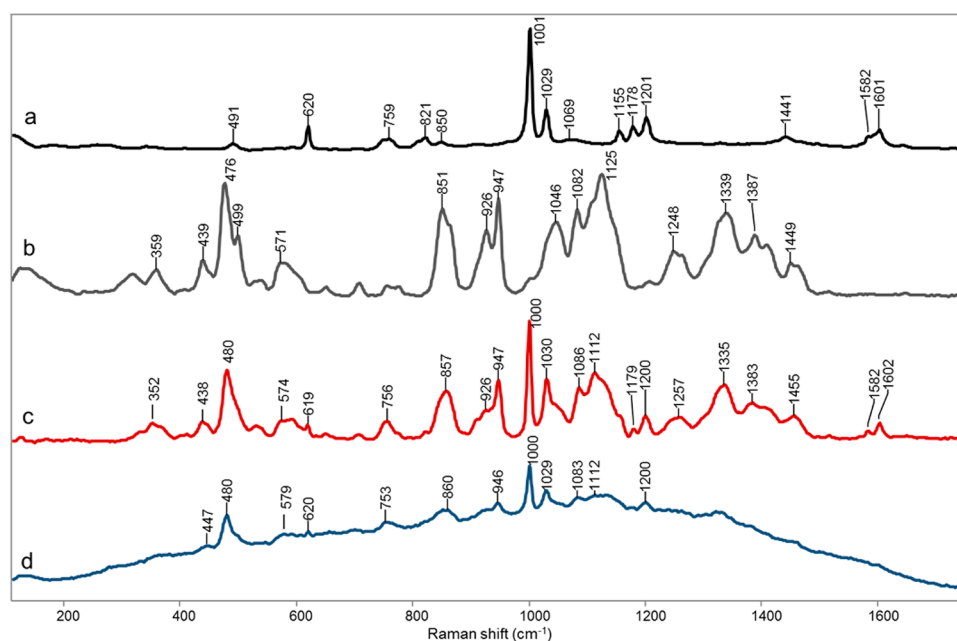**Figure 9.** IR spectra of (a) PhEA, (b) βCD, (c) βCD-PhEA, and (d) βCD-PhEA with AuNPs.

Figure 10. Raman spectra of (a) PhEA, (b) βCD, (c) βCD-PhEA, and (d) βCD-PhEA with AuNPs.

due to the partial displacement of the guest toward the outside of βCD in the presence of the AuNPs.

Raman spectra can also be used to study the behavior of the guest compound in the IC (Figure 10). Furthermore, the addition of AuNPs enhances the signal of the system because of a phenomenon called surface-enhanced Raman scattering (SERS) that is produced when the molecule is close to silver and gold nanoparticles.[66,67] In this case, evidence of SERS in the spectrum with AuNPs (Figure 10, trace d) is given by the fact that the power was reduced to acquire that spectrum, still obtaining a significant signal.

In Figure 10, trace a shows the Raman spectrum of PhEA with its characteristic bands. The band at 491 cm^{-1} corresponds to a C−C−N scissoring, and the mode at 620 cm^{-1} is a phenyl ring in-plane deformation, and while it is faint, it can be observed in the inclusion compound (trace c) as well as in the SERS spectrum (trace d). The band at 759 cm^{-1} is an aromatic C−H bending and ring bending. The band at 821 cm^{-1} is a CH$_2$ rocking and NH$_2$ wagging, and the next band at 850 cm^{-1} is another NH$_2$ wagging. The most prominent band at 1001 cm^{-1} is the typical phenyl ring breathing, followed by another ring stretching at 1029 cm^{-1}. These two bands are conserved in the normal Raman spectrum of the IC (trace c) as well as in the SERS (trace d). A very faint band at 1069 cm^{-1} is assigned to a C−N stretching. The following bands at 1155 and 1178 cm^{-1} correspond to aromatic C−H bending, and the band at 1201 cm^{-1} is a C−C stretching mode between the phenyl ring and the ethyl moiety. This band can also be identified in the spectrum of the IC and in the SERS. The band at 1441 cm^{-1} corresponds to ethyl CH$_2$ scissoring vibrations, and the band at 1601 cm^{-1} is a ring in-plane deformation. The bands above 2700 cm^{-1} are very faint and not shown here (the full spectra can be found in the Supporting Information, section S6). When adding AuNPs, the bands that obtain the most SERS enhancement are those of the phenyl ring, rather than the amino group, both being close to the gold surface. This is because the bands of the amino group are not the most intense due to having relatively low polarizability compared to the phenyl ring vibrations. The interaction of the amino group with

the gold surface could not be inferred from the SERS data alone, as there is no additional enhancement. However, this interaction has been described previously, with the N−H bands disappearing from the IR spectrum,[59,97] which was also observed in the IR, Raman and SERS spectra.

The SERS experiment shows more prominently the bands of PhEA, rather than the bands of βCD, a much larger molecule having a larger cross-section. This result supports the idea of PhEA in the IC being closer to the nanoparticle than the βCD molecule.

Quantification of Gold Content, βCD, and PhEA in the Crystals of the IC. The percentage of gold in the samples with 20 s of sputtering was 0.673% (σ 0.016), a value higher than indicated by the EDX analysis. On the other hand, considering a stoichiometric ratio of 1:1, the mass fractions for each component in the complex and the gold content in the sample, the percentages of βCD and PhEA were 89.4% and 9.93%, respectively (see calculations in Supporting Information, section S7).

Drug-Loading Ability of the System in Solution. To evaluate the percentage of PhEA loaded with AuNPs, a component separation was performed. The excess of the complex in aqueous solution that is not interacting with the AuNPs was separated by centrifugation from the ternary system and was quantitated using UV−vis spectroscopy. The percentage of drug loaded in the ternary system (βCD-PhEA-AuNPs) corresponds to 71% with respect to the total content of PhEA; while 24% of the PhEA remains in the complex but without interacting with nanoparticles; and the remaining 5% of the PhEA is free due to dissociation from the matrix (see calculations in Supporting Information, section S7).

A schematic representation of the process of solubilization of the ternary system is shown in Figure 11. The AuNPs are formed by sputtering onto the crystals of βCD-PhEA (left) and then in the process of solubilization the IC molecules complete the capping of the nanoparticles surface (right).

Analysis of Drug Release by Laser Irradiation. A two-phase system was designed: an aqueous phase that contained the inclusion complex with AuNPs and an organic phase of
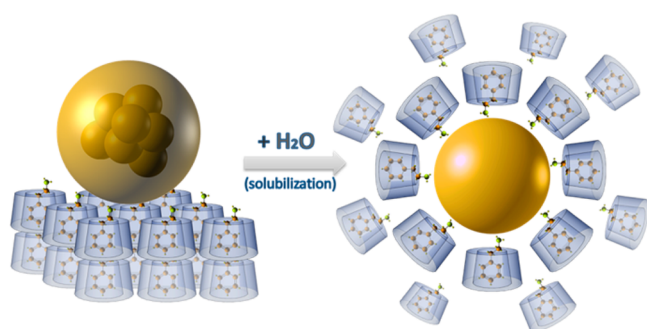
Figure 11. Schematic representation of the ternary system: in solid state with AuNPs onto crystals of the IC (left); and in solution with AuNPs coated by molecules of the IC.

chloroform, where the drug was expected to migrate following laser irradiation. AuNPs conjugated with ICs in aqueous solution were irradiated using a continuous laser at 532 nm, generating local heat and the release of PhEA molecules toward the organic phase. The absorbance of PhEA was measured using UV−visible spectroscopy in chloroform. The assays were conducted over 15, 30, 60, 90, or 120 min and compared with the maximum concentration of drug that was added (Figure 12a). The βCD-PhEA-AuNPs system irradiated for 60 min was compared with three other assays evaluated for the same time. The first assay corresponds to the βCD-PhEA complex evaluated without irradiation, the second assay corresponds to the complex with AuNPs and without irradiation, and the third assay corresponds to the irradiation of the βCD-PhEA complex without AuNPs. All assays were analyzed in comparison with the maximum concentration of drug that was added (Figure 12b).

The absorbance of PhEA was observed from the start (15 min). This implies that the drug is transferred to the organic phase gradually. A high absorbance was observed at 60 min, which was concluded to be the optimum time, and thereafter, the absorbance moderately increased. Assays without irradiation for βCD-PhEA complexes with and without AuNPs were conducted to observe whether the drug migrated to the organic phase independently. Unirradiated complexes released a portion of the drug, which was attributed to the chemical equilibrium of the system in solution; that is, this balance is interrupted by the presence of AuNPs, which maintain PhEA molecules in the aqueous phase (see AuNP with/non irradiated

in Figure 12). Assays with up to 60 min of irradiation of the complexes without AuNPs showed reduced absorbance compared with the irradiated ternary system, demonstrating with certainty that the photothermal effect caused by AuNPs promotes the release of PhEA from the ternary system more efficiently.

4. CONCLUSIONS

In summary, a crystalline solid of βCD-PhEA complex may be formed reproducibly in a molar ratio of 1:1. The ordered crystalline structure shows it to be an optimal substrate for the formation of AuNPs homogeneous in size using magnetron sputtering allowing the formation of the ternary system (βCD-PhEA-AuNPs) that remains stable in aqueous solution. Due to the Au−NH$_2$ interaction, the guest molecule in the ternary system is displaced partially toward the outside of βCD via the narrowest cavity; nevertheless, the aromatic ring remains inside the cavity of the matrix. The system in aqueous solution shows a high loading ability of PhEA. Furthermore, this new system of βCD-PhEA-AuNPs in aqueous solution enables the release of guest PhEA efficiently after irradiation with a continuous laser.

We believe that this unique system with two components (AuNPs and βCD) may be useful as a nanocarrier for different drugs. With respect to PhEA, these properties may result in an increase in the concentration of the psychoactive agent in the target action site with its effective release.

■ ASSOCIATED CONTENT

ⓢ Supporting Information

Network parameters obtained for the complexes with and without AuNPs by powder X-ray diffraction. ^{1}H-NMR spectrum for pure βCD, pure PhEA, βCD-PhEA, and βCD-PhEA-AuNPs in DMSO-d_6. The stoichiometry of the βCD-PhEA complex. Stability constant of the complex in aqueous solution. TEM images of AuNPs. Comparison between the calculated and experimental spectra of PhEA by IR and Raman spectroscopy. Quantification of gold content, βCD, and PhEA in the crystals of the IC. Drug-loading ability of the system in solution. The Supporting Information is available free of charge on the ACS Publications website at DOI: 10.1021/acsami.5b00186.
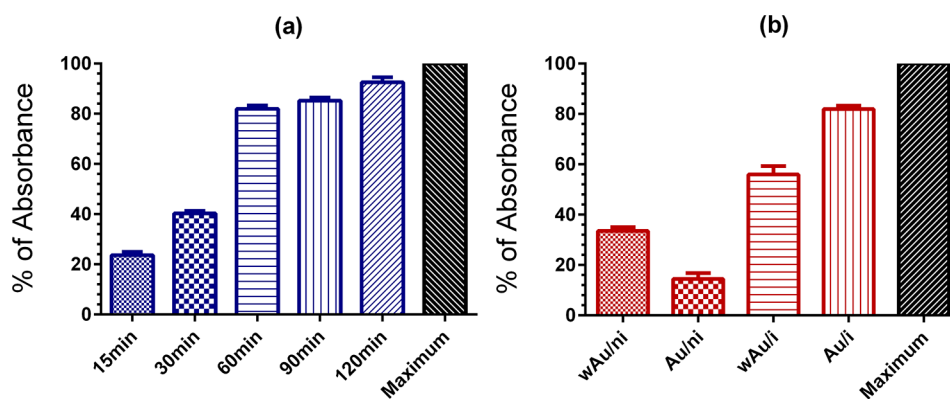

Figure 12. (a) Absorption percentages for PhEA at 258 nm in chloroform after different periods of irradiation ($n = 3$). (b) Absorption percentages for PhEA in four different systems for 60 min wAu/ni: without AuNPs, no irradiation; Au/ni: with AuNPs, no irradiation; wAu/i: without AuNPs, irradiation; Au/i: with AuNPs, irradiation. The maximum corresponds to the total of PhEA loaded for each test ($n = 3$).

AUTHOR INFORMATION

Corresponding Authors
*E-mail: mkogan@ciq.uchile.cl. Fax: 56 02 2713888.
*E-mail: nyutroni@uchile.cl.

Notes
The authors declare no competing financial interest.

REFERENCES

(1) Connors, K. A. The Stability of Cyclodextrin Complexes in Solution. *Chem. Rev.* **1997**, *97*, 1325−1357.

(2) Szejtli, J. Introduction and General Overview of Cyclodextrin Chemistry. *Chem. Rev.* **1998**, *98*, 1743−1753.

(3) Schneider, H. J.; Hacket, F.; Rudiger, V. NMR Studies of Cyclodextrins and Cyclodextrin Complexes. *Chem. Rev.* **1998**, *98*, 1755−1785.

(4) Davis, M. E.; Brewster, M. E. Cyclodextrin-Based Pharmaceutics: Past, Present and Future. *Nat. Rev. Drug Discovery* **2004**, *3*, 1023−1035.

(5) Del Valle, E. M. M. Cyclodextrins and their Uses: a Review. *Process Biochem.* **2004**, *39*, 1033−1046.

(6) Chen, M.; Diao, G.; Zhang, E. Study of Inclusion Complex of β-Cyclodextrin and Nitrobenzene. *Chemosphere* **2006**, *63*, 522−529.

(7) Aree, R.; Chaichit, N. Crystal Structure of β-Cyclodextrin-Benzoic Acid Inclusion Complex. *Carbohydr. Res.* **2003**, *338*, 439−446.

(8) Linde, G. A.; Laverde-Junior, A.; Vaz de Faria, E.; Barros-Colauto, N.; Faria de Moraes, F.; Zanin, G. M. The Use of 2D NMR to Study β-Cyclodextrin Complexation and Debittering of Amino Acids and Peptides. *Food Res. Int.* **2010**, *43*, 187−192.

(9) Manolikar, M. K.; Sawant, M. R. Study of Solubility of Isoproturon by its Complexation with β-Cyclodextrin. *Chemosphere* **2003**, *51*, 811−816.

(10) Hirayama, F.; Uekama, K. Cyclodextrin-Based Controlled Drug Release System. *Adv. Drug Delivery Rev.* **1999**, *36*, 125−141.

(11) Oda, M.; Kobayashi, M.; Aungst, B. J. β-Cyclodextrin as a Suitable Solubilizing Agent for *in situ* Absorption Study of Poorly Water-Soluble Drugs. *Int. J. Pharm.* **2004**, *280*, 95−102.

(12) Uekama, K.; Hirayama, F.; Arima, H. Recent Aspect of Cyclodextrin-Based Drug Delivery System. *J. Inclusion Phenom. Macrocyclic Chem.* **2006**, *56*, 3−8.

(13) Loftsson, T.; Duchene, D. Cyclodextrins and their Pharmaceutical Applications. *Int. J. Pharm.* **2007**, *329*, 1−11.

(14) Loftsson, T.; Brewster, M. Pharmaceutical Applications of Cyclodextrins: Basic Science and Product Development. *J. Pharm. Pharmacol.* **2010**, *62*, 1607−1621.

(15) Carrier, R. L.; Miller, L. A.; Ahmed, I. The Utility of Cyclodextrins for Enhancing Oral Bioavailability. *J. Controlled Release* **2007**, *123*, 78−99.

(16) Arun, R.; Kumar, C. K.; Sravanthi, V. V. N. S. S. Cyclodextrins as Drug Carrier Molecule: A Review. *Sci. Pharm.* **2008**, *76*, 567−598.

(17) Laza-Knoerr, A. L. Cyclodextrins for Drug Delivery. *J. Drug Targeting* **2010**, *18*, 645−656.

(18) Li, R. Q.; Niu, Y. L.; Zhao, N. N.; Yu, B. R.; Mao, C.; Xu, F. J. Series of New β-Cyclodextrin-Cored Starlike Carriers for Gene Delivery. *ACS Appl. Mater. Interfaces* **2014**, *6*, 3969−3978.

(19) Stella, V.; He, Q. Cyclodextrins. *Toxicol. Pathol.* **2008**, *36*, 30−42.

(20) Liu, B. Therapeutic Potential of Cyclodextrins in the Treatment of Niemann−Pick type C disease. *J. Clin. Lipidol.* **2012**, *7*, 289−301.

(21) Ottinger, E.; Kao, M.; Carrillo-Carrasco, N.; Yanjanin, N.; Kanakatti, R.; Janssen, M.; Brewster, M.; Scott, I.; Xu, X.; Cradock, J.; Terse, P.; Dehdashti, S.; Marugan, J.; Zheng, W.; Portilla, L.; Hubbs, A.; Pavan, W.; Heiss, J.; Vite, C.; Walkley, S.; Ory, D.; Silber, S.; Porter, F.; Austin, C.; McKew, J. Collaborative Development of 2-Hydroxypropyl-β-Cyclodextrin for the Treatment of Niemann-Pick Type C1 Disease. *Curr. Top. Med. Chem. (Sharjah, United Arab Emirates)* **2014**, *14*, 330−339.

(22) Vite, C.; Bagel, J.; Swain, G.; Prociuk, M.; Sikora, T.; Stein, V.; O'Donnell, P.; Ruane, T.; Ward, S.; Crooks, A.; Li, S.; Mauldin, E.; Stellar, S.; De Meulder, M.; Kao, M.; Ory, D.; Davidson, C.; Vanier, M.; Walkley, S. Intracisternal Cyclodextrin Prevents Cerebellar Dysfunction and Purkinje Cell Death in Feline Niemann-Pick Type C1 disease. *Sci. Transl. Med.* **2015**, *7*, 276ra26.

(23) Adeli, M.; Sadeghi, R.; Yadollahi, R.; Mahmoudib, M.; Kalantaria, M. Polyrotaxane/Gold Nanoparticle Hybrid Nanomaterials as Anticancer Drug Delivery Systems. *J. Mater. Chem.* **2011**, *21*, 18686−18695.

(24) Shi, Y.; Goodisman, J.; Dabrowiak, J. Cyclodextrin Capped Gold Nanoparticles as a Delivery Vehicle for a Prodrug of Cisplatin. *Inorg. Chem.* **2013**, *52*, 9418−9426.

(25) Park, C.; Youn, H.; Kim, H.; Noh, T.; Hee, Y.; Tax, E.; Joo, H.; Kim, C. Cyclodextrin-Covered Gold Nanoparticles for Targeted Delivery of an Anti-Cancer Drug. *J. Mater. Chem.* **2009**, *19*, 2310−2315.

(26) Suzuki, O.; Katsumata, Y.; Oya, M. Oxidation of β-Phenyl-ethylamine by Both Types of Monoamine Oxidase: Examination of Enzymes in Brain and Liver Mitochondria of Eight Species. *J. Neurochem.* **1981**, *36*, 1298−1301.

(27) Sabelli, H.; Javaid, J. Phenylethlyamine Modulation of Affect: Therapeutic and Diagnostic Implications. *J. Neuropsychiatry Clin. Neurosci.* **1995**, *7*, 6−14.

(28) Sabelli, H.; Fink, P.; Fawcett, J.; Tom, C. Sustained Antidepressant Effects of PEA Replacement. *J. Neuropsychiatry Clin. Neurosci.* **1996**, *8*, 168−171.

(29) Szabo, A.; Billett, E.; Turner, J. Phenylethylamine, a Possible Link to the Antidepressant Effects of Exercise? *Br. J. Sports Med.* **2001**, *35*, 342−343.

(30) Daniel, M.; Astruc, D. Gold Nanoparticles: Assembly, Supramolecular Chemistry, Quantum-Size-Related Properties, and Applications toward Biology, Catalysis, and Nanotechnology. *Chem. Rev.* **2004**, *104*, 293−346.

(31) Chen, M. C.; Yang, Y. L.; Chen, S. W.; Li, J. H.; Aklilu, M.; Tai, Y. Self-Assembled Monolayer Immobilized Gold Nanoparticles for Plasmonic Effects in Small Molecule Organic Photovoltaic. *ACS Appl. Mater. Interfaces* **2013**, *5*, 511−517.

(32) Lance, K.; Coronado, E.; Zhao, L.; Schatz, G. C. The Optical Properties of Metal Nanoparticles: The Influence of Size, Shape, and Dielectric Environment. *J. Phys. Chem. B* **2003**, *107*, 668−677.

(33) Mock, J.; Smith, D.; Schultz, S. Local Refractive Index Dependence of Plasmon Resonance Spectra from Individual Nanoparticles. *Nano Lett.* **2003**, *3*, 485−491.

(34) Su, K.; Wei, Q.; Zhang, X. Interparticle Coupling Effects on Plasmon Resonances of Nanogold Particles. *Nano Lett.* **2003**, *3*, 1087−1090.

(35) Okamoto, T.; Yamaguchi, I. Optical Absorption Study of the Surface Plasmon Resonance in Gold Nanoparticles Immobilized onto a Gold Substrate by Self-Assembly Technique. *J. Phys. Chem. B* **2003**, *107*, 10321−10324.

(36) Brigger, I.; Dubernet, C.; Couvreur, P. Nanoparticles in Cancer Therapy and Diagnosis. *Adv. Drug Delivery Rev.* **2002**, *54*, 631−651.

(37) Jong, W.; Borm, P. Drug Delivery and Nanoparticles: Applications and Hazards. *Int. J. Nanomed.* **2008**, *3*, 133−149.

(38) Feng, X.; Lv, F.; Liu, L.; Tang, H.; Xing, C.; Yang, Q.; Wang, S. Conjugated Polymer Nanoparticles for Drug Delivery and Imaging. *ACS Appl. Mater. Interfaces* **2010**, *2*, 2429−2435.

(39) Ghosh, P.; Han, G.; De, M.; Kim, C. K.; Rotello, V. M. Gold Nanoparticles in Delivery Applications. *Adv. Drug Delivery Rev.* **2008**, *60*, 1307−1315.

(40) Shaji, J.; Lal, M. Nanocarriers for Targeting in Inflammation. *Asian J. Pharm. Clin. Res.* **2013**, *6*, 3−12.

(41) Bertrand, N.; Wu, j.; Xu, X.; Kamaly, N.; Farokhzad, O. Cancer Nanotechnology: The Impact of Passive and Active Targeting in the Era of Modern Cancer Biology. *Adv. Drug Delivery Rev.* **2014**, *66*, 2−25.

(42) Nehoff, H.; Parayath, H.; Domanovitch, L.; Taurin, S.; Greish, K. Nanomedicine for Drug Targeting: Strategies Beyond the Enhanced Permeability and Retention Effect. *Int. J. Nanomed.* **2014**, *9*, 2539−2555.

(43) Kobayashi, H.; Watanabe, R.; Choyke, P. Improving Conventional Enhanced Permeability and Retention (EPR) Effects; What Is the Appropriate Target? *Theranostics* **2014**, *4*, 81−89.

(44) Lasagna-Reeves, C.; Gonzalez-Romero, D.; Barria, M. A.; Olmedo, I.; Clos, A.; Sadagopa, V. M.; Urayama, A.; Vergara, L.; Kogan, M. J.; Soto, C. Bioaccumulation and Toxicity of Gold Nanoparticles after Repeated Administration in Mice. *Biochem. Biophys. Res. Commun.* **2010**, *393*, 649−655.

(45) Guerrero, S.; Araya, E.; Fiedler, J. L.; Arias, J. I.; Adura, C.; Albericio, F.; Giralt, E.; Fernández, M. S.; Kogan, M. J. Improving the Brain Delivery of Gold Nanoparticles by Conjugation with an Amphipathic Peptide. *Nanomedicine* **2010**, *5*, 897−913.

(46) Prades, R.; Guerrero, S.; Araya, E.; Molina, C.; Salas, E.; Zurita, E.; Selva, J.; Egea, G.; López-Iglesias, C.; Teixidó, M.; Kogan, M.; Giralt, E. Delivery of Gold Nanoparticles to the Brain by Conjugation with a Peptide that Recognizes the Transferrin Receptor. *Biomaterials* **2012**, *33*, 7194−7205.

(47) Bansal, S. R.; Chaudhary, M.; Basu, A.; Bhonde, R. R.; Sastry, M. Biocompatibility of Gold Nanoparticles and their Endocytotic Fate inside the Cellular Compartment: A Microscopic Overview. *Langmuir* **2005**, *21*, 10644−10654.

(48) Sonavane, G.; Tomoda, K.; Makino, K. Biodistribution of Colloidal Gold Nanoparticles after Intravenous Administration: Effect of Particle Size. *Colloids Surf., B* **2008**, *66*, 274−280.

(49) Wang, L.; Li, Y. F.; Liu, Y.; Meng, L.; Zhang, K.; Wu, X.; Zhang, L.; Li, B.; Chen, C. Characterization of Gold Nanorods *in vivo* by Integrated Analytical Techniques: Their Uptake, Retention, and Chemical Forms. *Anal. Bioanal. Chem.* **2010**, *396*, 1105−1114.

(50) Dykman, L.; Khlebtsov, N. Gold Nanoparticles in Biomedical Applications: Recent Advances and Perspectives. *Chem. Soc. Rev.* **2012**, *41*, 2256−2282.

(51) Yen, H. J.; Hsu, S. H.; Tsai, C. L. Cytotoxicity and Immunological Response of Gold and Silver Nanoparticles of Different Sizes. *Small* **2009**, *5*, 1553−1561.

(52) Tirelli, N. (Bio)Responsive Nanoparticles. *Curr. Opin. Colloid Interface Sci.* **2006**, *11*, 210−216.

(53) Connor, E. E.; Mwamuka, J.; Gole, A.; Murphy, C. J.; Wyatt, M. D. Gold Nanoparticles are Taken Up by Human Cells but do not Cause Acute Cytotoxicity. *Small* **2005**, *1*, 325−327.

(54) Pan, Y.; Neuss, S.; Leifert, A.; Fischler, M.; Wen, F.; Simon, U.; Schmid, G.; Brandau, W.; Jahnen-Dechent, W. Size-Dependent Cytotoxicity of Gold Nanoparticles. *Small* **2007**, *3*, 1941−1949.

(55) Gibson, J. D.; Khanal, B. P.; Zubarev, E. R. Paclitaxel-Functionalized Gold Nanoparticles. *J. Am. Chem. Soc.* **2007**, *129*, 11653−11661.

(56) Colleen, M. A.; James, C. D.; Mathew, M. M. Investigation of the Drug Binding Properties and Cytotoxicity of DNA-Capped Nanoparticles Designed as Delivery Vehicles for the Anticancer Agents Doxorubicin and Actinomycin D. *Bioconjugate Chem.* **2012**, *23*, 2061−2070.

(57) Adura, C.; Guerrero, S.; Salas, E.; Medel, L.; Riveros, A.; Mena, J.; Arbiol, J.; Albericio, F.; Giralt, E.; Kogan, M. J. Stable Conjugates of Peptides with Gold Nanorods for Biomedical Applications with Reduced Effects on Cell Viability. *ACS Appl. Mater. Interfaces* **2013**, *5*, 4076−4085.

(58) Kumar, S.; Gandhi, K.; Kumar, R. Modeling of Formation of Gold Nanoparticles by Citrate Method. *Ind. Eng. Chem. Res.* **2007**, *46*, 3128−3136.

(59) Sperling, R.; Parak, W. Surface Modification, Functionalization and Bioconjugation of Colloidal Inorganic Nanoparticles. *Philos. Trans. R. Soc., A* **2010**, *368*, 1333−1383.

(60) Schulz, F.; Homolka, T.; Bastús, N.; Puntes, V.; Weller, H.; Vossmeyer, T. Little Adjustments Significantly Improve the Turkevich Synthesis of Gold Nanoparticles. *Langmuir* **2014**, *30*, 10779−10784.

(61) Barrientos, L.; Yutronic, N.; del Monte, F.; Gutiérrez, M. C.; Jara, P. Ordered Arrangement of Gold Nanoparticles on an α-Cyclodextrin−Dodecanethiol Inclusion Compound Produced by Magnetron Sputtering. *New J. Chem.* **2007**, *31*, 1400−1402.

(62) Rodriguez-Llamazares, S.; Jara, P.; Yutronic, N.; Noyong, M.; Bretschneider, J.; Simon, U. Face Preferred Deposition of Gold Nanoparticles on α-Cyclodextrin/Octanethiol Inclusion Compound. *J. Colloid Interface Sci.* **2007**, *316*, 202−205.

(63) Barrientos, L.; Yutronic, N.; Muñoz, M.; Silva, N.; Jara, P. Metallic Nanoparticle Tropism of Alkylthiol Guest Molecules Included into α-Cyclodextrin Host. *Supramol. Chem.* **2009**, *21*, 264−267.

(64) Herrera, B.; Adura, C.; Yutronic, N.; Kogan, M. J.; Jara, P. Selective Nanodecoration of Modified Cyclodextrin Crystals with Gold Nanorods. *J. Colloid Interface Sci.* **2013**, *389*, 42−45.

(65) Campos, C.; Muñoz, M.; Barrientos, L.; Lang, E.; Jara, P.; Sobrados, I.; Yutronic, N. Adhesion of Gold and Silver Nanoparticles onto Urea−Alkylamine Inclusion Compounds. *J. Inclusion Phenom. Macrocyclic Chem.* **2013**, *75*, 165−173.

(66) Aroca, R. The Interaction of Light with Nanoscopic Metal Particles and Molecules on Smooth Reflecting Surfaces. *In Surface-Enhanced Vibrational Spectroscopy*; John Wiley and Sons: Chichester, 2006; Chapter 2, pp 35−71.

(67) Le Ru, E.; Etchegoin, P. Introduction to Plasmons and Plasmonics. In *Principles of Surface Enhanced Raman Spectroscopy (and Related Plasmonic Effects)*; Elsevier: Amsterdam, The Netherlands, 2009; Chapter 3, pp 121−183.

(68) Huang, X.; Jain, P. K.; El-Sayed, I. H.; El-Sayed, M. A. Plasmonic Photothermal Therapy (PPTT) Using Gold Nanoparticles. *Lasers Med. Sci.* **2008**, *23*, 217−228.

(69) Guerrero, A. R.; Hassan, N.; Escobar, C. A.; Albericio, F.; Kogan, M.j.; Araya, E. Gold Nanoparticles for Photothermally Controlled Drug Release. *Nanomedicine (London, U. K.)* **2014**, *13*, 2023−2029.

(70) Etheridge, M.; Campbell, S.; Erdman, A.; Haynes, C.; Wolf, S.; Mccullough, J. The Big Picture on Nanomedicine: The State of Investigational and Approved Nanomedicine Products. *Nanomedicine (N. Y., NY, U. S.)* **2013**, *9*, 1−14.

(71) Libutti, S.; Paciotti, G.; Byrnes, A.; Alexander, H.; Gannon, W.; Walker, M.; Seidel, G.; Yuldasheva, N.; Tamarkin, L.; Phase, I. and Pharmacokinetic Studies of CYT-6091, a Novel PEGylated Colloidal Gold-rhTNF Nanomedicine. *Clin. Cancer Res.* **2010**, *16*, 6139−6149.

(72) Liu, Y.; Male, K.; Bouvrette, P.; Luong, J. Control of the Size and Distribution of Gold Nanoparticles by Unmodified Cyclodextrins. *Chem. Mater.* **2003**, *15*, 4172−4180.

(73) Kabashin, A.; Meunier, M.; Kingston, C.; Luong, J. Fabrication and Characterization of Gold Nanoparticles by Femtosecond Laser Ablation in an Aqueous Solution of Cyclodextrins. *J. Phys. Chem. B* **2003**, *107*, 4527−4531.

(74) Sylvestre, J.; Kabashin, A.; Sacher, E.; Meunier, M.; Luong, J. Stabilization and Size Control of Gold Nanoparticles during Laser Ablation in Aqueous Cyclodextrins. *J. Am. Chem. Soc.* **2004**, *126*, 7176−7177.

(75) Gimenez, L.; Anazetti, M.; Melo, P.; Haun, M.; De Azevedo, M.; Durán, N.; Alves, O. Cytotoxicity on V79 and HL60 Cell Lines by Thiolated-β-Cyclodextrin-Au/Violacein Nanoparticles. *J. Biomed. Nanotechnol.* **2005**, *1*, 1−7.

(76) Tang, B.; Cao, L.; Xu, K.; Zhuo, L.; Ge, J.; Li, Q.; Yu, L. A New Nanobiosensor for Glucose with High Sensitivity and Selectivity in Serum Based on Fluorescence Resonance Energy Transfer (FRET) between CdTe Quantum Dots and Au Nanoparticles. *Chem.—Eur. J.* **2008**, *14*, 3637−3644.

(77) Li, X.; Qi, Z.; Liang, K.; Bai, X.; Xu, J.; Liu, J.; Shen, J. An Artificial Supramolecular Nanozyme Based on β-Cyclodextrin-Modified Gold Nanoparticles. *Catal. Lett.* **2008**, *124*, 413−417.

(78) Frisch, M. J.; Trucks, G. W.; Schlegel, H. B.; Scuseria, G. E.; Robb, M. A.; Cheeseman, J. R.; Scalmani, G.; Barone, V.; Mennucci, B.; Petersson, G. A.; Nakatsuji, H.; Caricato, M.; Li, X.; Hratchian, H. P.; Izmaylov, A. F.; Bloino, J.; Zheng, G.; Sonnenberg, J. L.; Hada, M.; Ehara, M.; Toyota, K.; Fukuda, R.; Hasegawa, J.; Ishida, M.; Nakajima, T.; Honda, Y.; Kitao, O.; Nakai, H.; Vreven, T.; Montgomery, J. A.; Peralta, Jr., J. E.; Ogliaro, F.; Bearpark, M.; Heyd, J. J.; Brothers, E.; Kudin, K. N.; Staroverov, V. N.; Kobayashi, R.; Normand, J.; Raghavachari, K.; Rendell, A.; Burant, J. C.; Iyengar, S. S.; Tomasi, J.; Cossi, M.; Rega, N.; Millam, J. M.; Klene, M.; Knox, J. E.; Cross, J. B.; Bakken, V.; Adamo, C.; Jaramillo, J.; Gomperts, R.; Stratmann, R. E.; Yazyev, O.; Austin, A. J.; Cammi, R.; Pomelli, C.; Ochterski, J. W.; Martin, R. L.; Morokuma, K.; Zakrzewski, V. G.; Voth, G. A.; Salvador, P.; Dannenberg, J. J.; Dapprich, S.; Daniels, A. D.; Farkas, Ö.; Foresman, J. B.; Ortiz, J. V.; Cioslowski, J.; Fox, D. J. *Gaussian 09*, revision D.01; Gaussian, Inc.: Wallingford, CT, 2009.

(79) Caira, M. R. On the Isostructurality of Cyclodextrin Inclusion Complexes and its Practical Utility. *Rev. Roum. Chim.* **2001**, *46*, 371−386.

(80) Dang, Z.; Song, L. X.; Quing, X.; Yun, F.; Yang, J.; Yang, J. Applications of Powder X-Ray Diffraction to Inclusion Complexes of Cyclodextrins. *Curr. Org. Chem.* **2011**, *15*, 848−861.

(81) Wang, E. J.; Lian, Z. X.; Cai, J. The Crystal Structure of the 1:1 Inclusion Complex of β-Cyclodextrin with Benzamide. *Carbohydr. Res.* **2007**, *342*, 767−771.

(82) Murugesan, M.; Cunningham, D.; Martinez-Albertos, J. L.; Vrcelj, R. M.; Moore, B. D. Nanoparticle-Coated Microcrystals. *Chem. Commun. (Cambridge, U. K.)* **2005**, 2677−2679.

(83) Fujiki, Y.; Takunaga, N.; Shinkai, S.; Sada, K. Anisotropic decoration of gold nanoparticles onto specific crystal faces of organic single crystals. *Angew. Chem., Int. Ed.* **2006**, *45*, 4764−4767.

(84) Nikolic, K.; Murugesan, M.; Forshaw, M.; Cunningham, D.; Martinez-Albertos, J.-L.; Moore, B. D. Self-assembly of Nanoparticles on the Surface of Ionic Crystals: Structural Properties. *Surf. Sci.* **2007**, *600*, 2730−2734.

(85) Barrientos, L.; Lang, E.; Zapata-Torres, G.; Celis-Barros, C.; Orellana, C.; Jara, P.; Yutronic, N. Structural Elucidation of Supramolecular Alpha-Cyclodextrin Dimer/Aliphatic Monofunctional Molecules Complexes. *J. Mol. Model.* **2013**, *19*, 2119−2126.

(86) Job, P. Formation and Stability of Inorganic Complexes in Solution. *Ann. Chim. (Rome, Italy)* **1928**, *9*, 113−203.

(87) Higuchi, T.; Connors, K. A. Phase Solubility Techniques. *Adv. Anal. Chem. Instrum.* **1965**, *4*, 117−122.

(88) Connors, K. A. The Stability of Cyclodextrin Complexes in Solution. *Chem. Rev.* **1997**, *97*, 1325−1357.

(89) Rao, V. M.; Stella, V. J. When can Cyclodextrins be Considered for Solubilizing Purposes. *J. Pharm. Sci.* **2003**, *92*, 927−932.

(90) Pessine, F.; Calderini, A.; Alexandrino, G. Review: Cyclodextrin Inclusion Complexes Probed by NMR Techniques. In *Magnetic Resonance Spectroscopy*; Kim, D., Ed.; InTech: Rijeka, Croatia, **2014**; Chapter 12, pp 237−265.

(91) Leyva, E.; Moctezuma, E.; Strouse, J.; García, M. Spectrometric and 2D NMR Studies on the Complexation of Chlorophenols with Cyclodextrins. *J. Inclusion Phenom. Macrocyclic Chem.* **2001**, *39*, 41−46.

(92) Mashhood, S.; Maheshwari, A.; Kumar, S.; Chun, K. High Resolution NMR Spectroscopic Study of Complexation of Hydroxyzine Hydrochloride with β-Cyclodextrin in Aqueous Solution. *J. Chin. Chem. Soc. (Peking)* **2006**, *53*, 867−871.

(93) Bergonzi, M.; Bilia, A. R.; Di Bari, L.; Mazzia, G.; Vincieri, F. Studies on the Interactions between some Flavonols and Cyclodextrins. *Bioorg. Med. Chem. Lett.* **2007**, *17*, 5744−5748.

(94) Voulgari, A.; Benaki, D.; Michaleas, S.; Antoniadou-Vyza, E. The Effect of β-Cyclodextrin on Tenoxicam Photostability, Studied by a New Liquid Chromatography Method; the Dependence on Drug Dimerisation. *J. Inclusion Phenom. Macrocyclic Chem.* **2007**, *57*, 141−146.

(95) Bisson-Boutelliez, C.; Fontanay, S.; Finance, C.; Kedzierewicz, F. Preparation and Physicochemical Characterization of Amoxicillin β-Cyclodextrin Complexes. *AAPS PharmSciTech* **2010**, *11*, 574−581.

(96) Jahed, V.; Zarrabi, A.; Bordbar, A.; Hafezi, M. NMR (1H, ROESY) Spectroscopic and Molecular Modelling Investigations of Supramolecular Complex of β-Cyclodextrin and Curcumin. *Food Chem.* **2014**, *165*, 241−246.

(97) Kumar, A.; Mandal, S.; Selvakannan, P.; Pasricha, R.; Mandale, A.; Sastry, M. Investigation into the Interaction between Surface-Bound Alkylamines and Gold Nanoparticles. *Langmuir* **2003**, *19*, 6277−6282.

(98) Leff, D. V.; Brandt, L.; Heath, J. R. Synthesis and Characterization of Hydrophobic, Organically-Soluble Gold Nanocrystals Functionalized with Primary Amines. *Langmuir* **1996**, *12*, 4723−4730.

(99) Sampaio, C.; Moriwaki, C.; Nogueira, A.; Sato, F.; Baesso, M.; Medina, A.; Matioli, G. Curcumin−β-Cyclodextrin Inclusion Complex: Stability, Solubility, Characterisation by FT-IR, FT-Raman, X-Ray Diffraction and Photoacoustic Spectroscopy, and Food Application. *Food Chem.* **2014**, *153*, 361−370.

(100) Pandian, K.; Mohamad, S.; Muhamad, N.; Atiqah, N. Synthesis and Characterization of the Inclusion Complex of β-Cyclodextrin and Azomethine. *Int. J. Mol. Sci.* **2013**, *14*, 3671−3682.

(101) Heise, H. M.; Kuchuk, R.; Bereck, A.; Riegel, D. Infrared Spectroscopy and Raman Spectroscopy of Cyclodextrin Derivatives and their Ferrocene Inclusion Complexes. *Vib. Spectrosc.* **2010**, *53*, 19−23.

(102) de Oliveira, V.; Almeida, E.; Castro, H.; Edwards, H.; Dos Santos, H.; de Oliveira, L. Carotenoids and β-Cyclodextrin Inclusion Complexes: Raman Spectroscopy and Theoretical Investigation. *J. Phys. Chem. A* **2011**, *115*, 8511−8519.